Quasiharmonic models for the calculation of thermodynamic properties of crystalline silicon under strain

H. Zhao and Z. Tang
Department of Mechanical and Industrial Engineering, University of Illinois at Urbana-Champaign, Urbana, Illinois 61801

G. Li
Beckman Institute for Advanced Science and Technology, University of Illinois at Urbana-Champaign, Urbana, Illinois 61801

N. R. Aluru[a)]
Department of Mechanical and Industrial Engineering, University of Illinois at Urbana-Champaign, Urbana, Illinois 61801

(Received 4 October 2005; accepted 1 February 2006; published online 31 March 2006)

Quasiharmonic models with Tersoff [Phys. Rev. B **38**, 9902 (1988)] interatomic potential are used to study the thermodynamic properties of crystalline silicon. It is shown that, compared to the molecular dynamics simulation data, the reciprocal space quasiharmonic model accurately predicts the thermal properties for temperatures up to 800 K. For higher temperatures, anharmonic effects become significant. With a significantly higher computational cost, the results from the real space quasiharmonic model approach the results from the reciprocal space quasiharmonic model as the number of atoms increases. The local quasiharmonic model does not accurately describe the thermal properties as it neglects the vibrational coupling of the atoms. We also investigate the effect of the strain on the thermodynamic properties. The variation of the thermodynamic properties with temperature under a tension, compression, and a shear deformation state is computed. © *2006 American Institute of Physics*. [DOI: 10.1063/1.2185834]

I. INTRODUCTION

Thermodynamic properties of crystalline silicon have long been a focus of interest because of their important role in elucidating the material behavior. Computational analysis is a powerful approach to investigate the thermodynamic properties of materials. First-principles quantum-mechanical methods are generally most accurate for predicting the material properties. *Ab initio* local density functional techniques have been used to determine the thermodynamic properties of silicon[1] and other materials.[2] However, due to the complexity of these methods and the need for large computational resources, *ab initio* calculations are limited to very small systems. Empirical and semi-empirical interatomic potentials[3–5] have been developed to provide a simpler and yet a reasonably accurate description of materials. The various parameters in these potentials are determined by a weighted fitting of the material property databases obtained from experiments or *ab initio* calculations. Molecular dynamics (MD) and Monte Carlo (MC) simulations are the two popular methods that are based on interatomic potentials. In these methods, the thermal statistics are gathered to calculate the ensemble average of the thermal properties. MD calculations on the thermodynamic properties of crystalline silicon were carried out in Ref. 6, where the Tersoff potential[4] was used. In Ref. 7, a Monte Carlo method was used to calculate the elastic properties of silicon by using both the Tersoff and the Stillinger-Weber[3] potentials. Despite their popularity, computational cost is still an inherent drawback with the MD and the MC methods.

Another class of methods relies on the theory of quantum-mechanical lattice dynamics, where the key step is the quasiharmonic approximation of the interatomic potential.[8,9] For a system of N atoms with a given interatomic potential, free energies and thermodynamic properties can be computed by diagonalizing a $3N\times 3N$ force constant matrix.[9] For a perfect crystal lattice, due to the periodicity of the atomic structure, it is more efficient to compute the relevant quantities in the reciprocal space.[9] As a further simplification of the quasiharmonic approximation, a local quasiharmonic approximation has been proposed[10] to reduce the $3N\times 3N$ eigenvalue problem for a system of N atoms to N 3×3 eigenvalue problems. In the local quasiharmonic approximation, it is assumed that the vibration of each atom in the system is independent of other atoms, i.e., we neglect all the terms in the quasiharmonic approximation that couple the vibrations of different atoms. These models based on the quasiharmonic approximation provide attractive alternatives for computational analysis of material properties. For example, along with the MD calculations, the quasiharmonic model in real space has been used in Ref. 6 to compute several thermodynamic properties of crystalline silicon. However, the questions on the accuracy and to what extent these models can describe the thermodynamic properties of silicon still remain. In this paper, we answer these questions by studying the bulk thermodynamic properties of crystalline silicon using three quasiharmonic models with the Tersoff interatomic potential: the quasiharmonic model in real space

[a)]Author to whom correspondence should be addressed; URL: http://www.uiuc.edu/~aluru; electronic mail: aluru@uiuc.edu;

(QHM), the quasiharmonic model in the reciprocal space or the **k**-space (QHMK), and the local quasiharmonic model (LQHM). The lattice constant, thermal expansion coefficient, Helmholtz free energy, entropy, internal energy, and heat capacity at constant volume are computed by using these three models and the results are compared with the MD simulation data given in Ref. 6. It is shown in the paper that the QHMK model accurately predicts the thermal properties for temperatures up to 800 K. For higher temperatures, anharmonic effects become significant. When a sufficient number of atoms are included (>216 atoms) in the QHM model, the difference between the results obtained from the QHMK and the QHM models is small. The computational cost of the QHM model, however, is much higher compared to that of the QHMK model. The LQHM model is inaccurate for many thermal properties, which indicates its limitation in predicting the material properties at finite temperature.

Due to the advances in micro- and nanotechnologies, silicon has been widely used to fabricate mechanical structures with applications in micro- and nanoelectromechanical systems.[11–13] Since the thermodynamic properties of silicon are closely related to the mechanical behavior of the silicon structure at finite temperature, it becomes necessary to investigate the thermodynamic properties of silicon under various strain conditions. In this paper, we investigate the strain effects on the thermal properties of Tersoff silicon by using the QHM and the QHMK models. In particular, we compute the thermal properties when the silicon crystal is subjected to a compression, stretch, and a shear deformation.

The rest of the paper is organized as follows: in Sec. II, the Tersoff potential and the quasiharmonic theories are introduced; in Sec. III, we compute the thermodynamic properties of a perfect silicon crystal by using the three quasiharmonic models and compare the results with the MD data given in the literature; the strain effect on the thermodynamic properties is presented in Sec. IV, and conclusions are given in Sec. V.

II. MODELS

A. Tersoff empirical potential

In the Tersoff empirical potential model,[4] the interatomic potential energy of a given system is expressed as the sum of local many-body interactions. The total potential energy U of a system is given by

$$U=\sum_{\alpha} U_{\alpha}=\frac{1}{2}\sum_{\alpha\neq\beta} V_{\alpha\beta}, \tag{1}$$

where α and β denote the atoms of the system and $V_{\alpha\beta}$ is the bond energy between atoms α and β and is given by

$$V_{\alpha\beta}=f_C(r_{\alpha\beta})[a_{\alpha\beta}f_R(r_{\alpha\beta})+b_{\alpha\beta}f_A(r_{\alpha\beta})], \tag{2}$$

where

$$f_C(r)=\begin{cases}1, & r<R_c-D\\ \frac{1}{2}-\frac{1}{2}\sin[\pi(r-R_c)/(2D)], & R_c-D\leqslant r\leqslant R_c+D\\ 0, & r>R_c+D,\end{cases}$$

$$f_R(r)=A\exp(-\lambda_1 r), \tag{3}$$

$$f_A(r)=-B\exp(-\lambda_2 r).$$

In Eqs. (2) and (3), $r_{\alpha\beta}$ is the bond length or the distance between atoms α and β, $f_C(r_{\alpha\beta})$ is a smooth cutoff function used to limit the range of the potential, R_c is the cutoff distance, D is another cutoff parameter which specifies the region around R_c where the cutoff function goes smoothly from 1 to 0, $f_R(r)$ is the repulsive pair potential, $f_A(r)$ is the attractive pair potential associated with bonding, and A, B, λ_1, and λ_2 are constants. $a_{\alpha\beta}$ is taken to be 1.0 for silicon. The function $b_{\alpha\beta}$ is a measure of the bond order which describes the dependence of the bond-formation energy on the local atomic arrangement due to the presence of other neighboring atoms, which is given by

$$b_{\alpha\beta}=(1+\mu^n\zeta_{\alpha\beta}^n)^{-1/2n},$$

$$\zeta_{\alpha\beta}=\sum_{\gamma\neq\alpha,\beta} f_C(r_{\alpha\gamma})g(\theta_{\alpha\beta\gamma})\exp[\lambda_3^3(r_{\alpha\beta}-r_{\alpha\gamma})^3], \tag{4}$$

$$g(\theta)=1+c^2/d^2-c^2/[d^2+(h-\cos\theta)^2],$$

where γ denotes an atom, $\zeta_{\alpha\beta}$ is called the effective coordination number, $\theta_{\alpha\beta\gamma}$ is the bond angle between the bonds $\alpha\beta$ and $\alpha\gamma$, and $g(\theta)$ is the stabilization function of the tetrahedral structure. The remaining variables are constant parameters which can be found in Table I of Ref. 4.

B. N-atom real space quasiharmonic (QHM) model

For an N-atom system, the Hamiltonian is given by[8]

$$H=\frac{1}{2}m\sum_{\alpha=1}^{N}\dot{\mathbf{v}}_{\alpha}^{T}\dot{\mathbf{v}}_{\alpha}+U(\mathbf{x}_1,\ldots,\mathbf{x}_N), \tag{5}$$

where m is the mass of the silicon atom, U is the total potential energy of the system, and $\mathbf{x}_\alpha$ and $\dot{\mathbf{v}}_\alpha$, $\alpha=1,\ldots,N$, are the position and the velocity vectors of atom α, respectively. The instantaneous position vector $\mathbf{x}_\alpha$ can be further written as

$$\mathbf{x}_{\alpha}=\mathbf{x}_{\alpha}^{0}+\mathbf{v}_{\alpha}, \tag{6}$$

where $\mathbf{x}_\alpha^0$ is the equilibrium position vector and $\mathbf{v}_\alpha$ is the displacement of atom α due to thermal vibration. In a harmonic approximation, the Tersoff potential function is written in a quadratic form by neglecting the higher-order (>2) terms in its Taylor's series expansion. The total potential energy can thus be rewritten as

$$U(\mathbf{x}_1,\ldots,\mathbf{x}_N)=U(\mathbf{x}_1^0,\ldots,\mathbf{x}_N^0)+\frac{1}{2}\sum_{\alpha,\beta=1}^{N}\sum_{j,k=1}^{3}\left.\frac{\partial^2 U(\mathbf{x}_1,\ldots,\mathbf{x}_N)}{\partial\mathbf{x}_{\alpha j}\partial\mathbf{x}_{\beta k}}\right|_{\mathbf{x}_1,\ldots,\mathbf{x}_N=\mathbf{x}_1^0,\ldots,\mathbf{x}_N^0}\mathbf{v}_{\alpha j}\mathbf{v}_{\beta k}, \tag{7}$$

where $\mathbf{x}_{\alpha j}$ and $\mathbf{x}_{\beta k}$ are the jth and the kth component of the position of atoms α and β, respectively, and $\mathbf{v}_{\alpha j}$ and $\mathbf{v}_{\beta k}$ are the jth and the kth component of the displacement of atoms α and β, respectively. Denoting $\mathbf{x}=(\mathbf{x}_1,\ldots,\mathbf{x}_N)$ and $\mathbf{x}^0=(\mathbf{x}_1^0,\ldots,\mathbf{x}_N^0)$, Eq. (7) can be rewritten in a matrix form as

$$U(\mathbf{x}) = U(\mathbf{x}^0) + \tfrac{1}{2}\mathbf{v}^T\mathbf{\Phi}\mathbf{v}, \tag{8}$$

where $\mathbf{v}=[\mathbf{v}_1,\ldots,\mathbf{v}_N]^T$ and $\mathbf{\Phi}$ is the $3N\times 3N$ force constant matrix given by

$$\Phi_{3\alpha+j-3,3\beta+k-3} = \left.\frac{\partial^2 U(\mathbf{x})}{\partial \mathbf{x}_{\alpha j}\partial \mathbf{x}_{\beta k}}\right|_{\mathbf{x}=\mathbf{x}^0}, \qquad \alpha,\beta = 1,\ldots,N, \quad j,k = 1,2,3. \tag{9}$$

Note that in the classical harmonic approximation, the force constant matrix is independent of temperature T, i.e., the equilibrium position $\mathbf{x}^0$ in Eq. (9) does not depend on temperature ($\mathbf{x}^0 \equiv \mathbf{x}^0|_{T=0}$). However, typically the volume of the crystal and the equilibrium position of the atoms, $\mathbf{x}^0$, vary with temperature. If the force constant matrix is allowed to change with the volume of the crystal, the harmonic approximation is then called the quasiharmonic approximation. Substituting Eq. (8) into the Hamiltonian, Eq. (5), one obtains

$$H = \tfrac{1}{2}m\dot{\mathbf{v}}^T\dot{\mathbf{v}} + \tfrac{1}{2}\mathbf{v}^T\mathbf{\Phi}\mathbf{v} + U(\mathbf{x}^0). \tag{10}$$

By diagonalizing the real symmetric force constant matrix $\mathbf{\Phi}$, Eq. (10) can be rewritten as

$$H = \tfrac{1}{2}m\dot{\mathbf{v}}^T\dot{\mathbf{v}} + \tfrac{1}{2}\mathbf{v}^T\mathbf{L}^T\mathbf{\Lambda}\mathbf{L}\mathbf{v} + U(\mathbf{x}^0), \tag{11}$$

where $\mathbf{\Lambda}$ is a $3N\times 3N$ real diagonal matrix whose entries $(\lambda_1,\lambda_2,\ldots,\lambda_{3N})$ are the eigenvalues of the force constant matrix $\mathbf{\Phi}$ and $\mathbf{L}$ is a $3N\times 3N$ orthogonal matrix ($\mathbf{L}^T\mathbf{L}=\mathbf{I}$) whose columns are the eigenvectors of $\mathbf{\Phi}$. Defining $\mathbf{q}=\mathbf{L}\mathbf{v}$ and $\dot{\mathbf{q}}=\mathbf{L}\dot{\mathbf{v}}$, Eq. (11) can be rewritten as

$$H = \tfrac{1}{2}m\dot{\mathbf{q}}^T\dot{\mathbf{q}} + \tfrac{1}{2}\mathbf{q}^T\mathbf{\Lambda}\mathbf{q} + U(\mathbf{x}^0), \tag{12}$$

where $\mathbf{q}$ and $\dot{\mathbf{q}}$ are the normal coordinates. Since the matrix $\mathbf{\Lambda}$ is diagonal, the Hamiltonian given in Eq. (12) can be rewritten as the sum of the energies of $3N$ independent harmonic oscillators in the normal coordinate system. For the jth harmonic oscillator, the Hamiltonian is given by

$$H_j = \tfrac{1}{2}m\dot{\mathbf{q}}_j^2 + \tfrac{1}{2}\lambda_j\mathbf{q}_j^2 + U_j(\mathbf{x}^0), \tag{13}$$

where $U_j(\mathbf{x}^0)$ is the potential energy for the jth oscillator at the equilibrium position. By solving the Schrödinger equation[14] for the harmonic oscillator given in Eq. (13), the energy levels of the jth harmonic oscillator are given by

$$\epsilon_{n,j} = U_j(\mathbf{x}^0) + \left(n+\frac{1}{2}\right)\hbar\omega_j, \qquad n = 0,1,2,\ldots, \quad j = 1,\ldots,3N, \tag{14}$$

where ω_j is the frequency of the jth oscillator given by

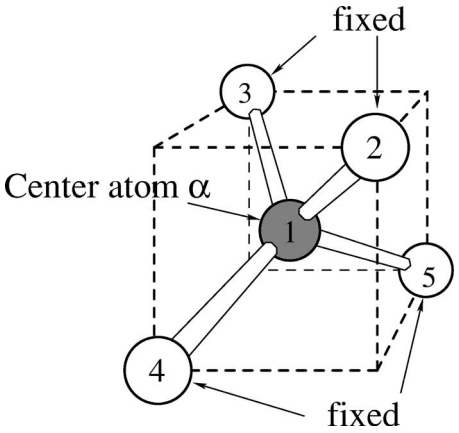

FIG. 1. The local quasiharmonic model.

$$\omega_j = \sqrt{\lambda_j/m}, \tag{15}$$

$\hbar$ is the reduced Planck's constant and n is the quantum number. Once the energy levels are obtained, the Helmholtz free energy A can be readily computed as[15]

$$A = -k_BT\sum_{j=1}^{3N}\ln\sum_{n=0}^{\infty}e^{-\epsilon_{n,j}/(k_BT)} = U(\mathbf{x}^0) + \frac{1}{2}\sum_{j=1}^{3N}\hbar\omega_j + k_BT\sum_{j=1}^{3N}\ln(1-e^{-\hbar\omega_j/(k_BT)}), \tag{16}$$

where k_B is the Boltzmann constant and T is the temperature. Note that on the right hand side of Eq. (16), the first term is the static lattice potential energy which is determined by the equilibrium positions of the atoms, the second term is the quantum-mechanical zero point energy, and the third term is the vibrational energy, which is a function of both the temperature and the atom positions. After the Helmholtz free energy is obtained, the internal energy E, the entropy S, and the heat capacity at constant volume, C_v, can be computed, as will be discussed in Sec. III.

C. Local quasiharmonic (LQHM) model

In the QHM model described in the previous section, the $3N\times 3N$ force constant matrix $\mathbf{\Phi}$ given in Eq. (9) must be diagonalized. If the system has a large number of atoms, i.e., N is large, the computational cost associated with solving the $3N\times 3N$ eigenvalue problem could be expensive. To overcome this difficulty, LeSar *et al.*[10] proposed a LQHM model. The main idea in the LQHM model is to assume that the vibration of each atom in the system is independent of other atoms and, hence, to neglect all terms in the QHM model that couple vibrations of different atoms. For each atom, a local 3×3 force constant matrix is constructed by fixing its neighboring atoms (Fig. 1) and the frequency of the center atom is computed by diagonalizing the local force constant matrix. In this section, the LQHM model is briefly reviewed in the context of calculating the thermodynamic properties of Tersoff silicon.

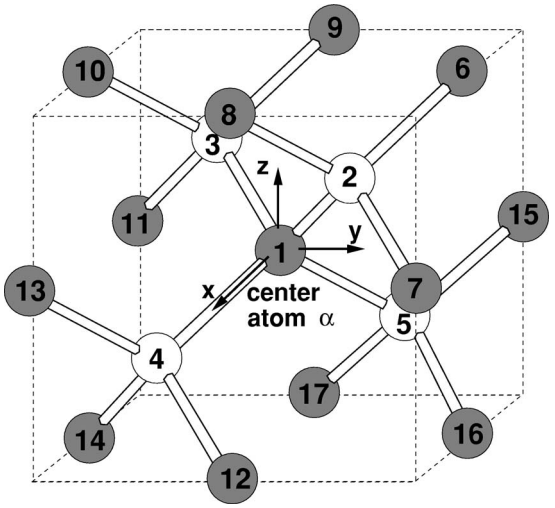

FIG. 2. Atom configuration and numbering for a center atom $\alpha \in B_1$.

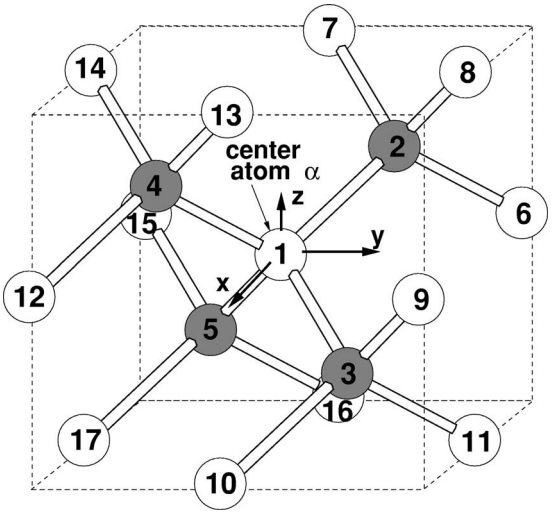

FIG. 3. Atom configuration and numbering for a center atom $\alpha \in B_2$.

In the LQHM model, the Hamiltonian of the center atom α is given by

$$H_\alpha = \frac{1}{2} m \dot{\mathbf{v}}_\alpha^T \dot{\mathbf{v}}_\alpha + \frac{1}{2} \mathbf{v}_\alpha^T \mathbf{\Phi}(\alpha) \mathbf{v}_\alpha + U_\alpha(\mathbf{x}^0), \tag{17}$$

where $U_\alpha(\mathbf{x}^0)$ is the potential energy of the center atom α at the equilibrium position, $\mathbf{v}_\alpha$ and $\dot{\mathbf{v}}_\alpha$ are 3×1 position and velocity vectors of the center atom α, respectively, and $\mathbf{\Phi}(\alpha)$ is the force constant matrix given by

$$\Phi_{j,k}(\alpha) = \left. \frac{\partial^2 U_{\text{local}}(\alpha)}{\partial \mathbf{x}_{\alpha j} \partial \mathbf{x}_{\alpha k}} \right|_{\mathbf{x}=\mathbf{x}^0}, \quad j,k = 1,2,3, \tag{18}$$

where $U_{\text{local}}(\alpha)$ is the local potential energy of atom α, which contains contributions from the first and the second nearest neighbors. In the LQHM model, the center atom α vibrates about its equilibrium position while the surrounding atoms are considered fixed. As shown in Fig. 1, the instantaneous position of the center atom ($\alpha=1$) affects the potential energy of atoms 1–5, i.e., the potential energy U_β, $\beta=1,\ldots,5$, is a function of the center atom position. Therefore, $U_{\text{local}}(\alpha)$ can be calculated within a cell that includes the first and the second nearest neighbors of the center atom (i.e., 17 atoms, as shown in Fig. 2). $U_{\text{local}}(\alpha)$ is given by

$$U_{\text{local}}(\alpha) = \sum_{\beta=1}^{5} U_\beta(\mathbf{x}_\sigma), \quad \alpha = 1, \quad \sigma \in \{1,\ldots,17\}, \tag{19}$$

where $\mathbf{x}_\sigma$ denotes the equilibrium position of atom β and its four neighbor atoms, and U_β is the potential energy of atom β. By following the same procedure outlined in Sec. II B, the energy levels of the center atom are given by

$$\epsilon_{n,j} = U_\alpha(\mathbf{x}^0) + \left(n + \frac{1}{2}\right)\hbar\omega_{\alpha j}, \qquad n = 0,1,2,\ldots, \quad j = 1,2,3, \tag{20}$$

where $\omega_{\alpha j}$ is the jth frequency of atom α. The Helmholtz free energy for an atom α in the LQHM approach is given by

$$A(\alpha) = U_\alpha(\mathbf{x}^0) + \frac{1}{2}\sum_{j=1}^{3} \hbar\omega_{\alpha j} + k_B T \sum_{j=1}^{3} \ln(1 - e^{-\hbar\omega_{\alpha j}/(k_B T)}). \tag{21}$$

The Helmholtz free energy for a perfect N-atom crystal is given by

$$A = \sum_{\alpha=1}^{N} A(\alpha). \tag{22}$$

As outlined above, the LQHM approach reduces the diagonalization of a $3N\times 3N$ force constant matrix to the diagonalization of N 3×3 matrices. For a system involving more than a few thousand atoms, the LQHM approach is considerably more efficient than the QHM approach.

D. Quasiharmonic model in the reciprocal space (QHMK)

As discussed in the previous sections, the size of the force constant matrix in the QHM approach is $3N\times 3N$, while the LQHM approach reduces the size of the force constant matrix to 3×3 by neglecting all terms in the QHM model that couple vibrations of different atoms. An alternative approach is the QHMK approach, which preserves the coupling of the vibrations of different atoms but significantly reduces the size of the force constant matrix. The key idea in the QHMK approach is to reduce the size of the force constant matrix based on the fact that the vibration of the atoms in a Bravais lattice has the same magnitude and direction and only differs in phase.[16] Before we express the Hamiltonian in the **k**-space, we introduce some notation for the silicon diamond structure, which contains two interpenetrating fcc Bravais lattices—denoted as B_1 and B_2. Figures 2 and 3 show the open and the shaded balls representing the two types of atoms belonging to the interpenetrating fcc Bravais lattices B_1 and B_2, respectively. Typically, for an N-atom silicon system, both B_1 and B_2 contain $N/2$ atoms. Figure 2 shows the atom configuration where the center atom α belongs to the

Bravais lattice B_1 and Fig. 3 shows the atom configuration where the center atom α belongs to the Bravais lattice B_2. The atom configuration shown in Fig. 3 is simply that shown in Fig. 2 with 90° rotation about the z-axis.

To express the Hamiltonian given in Eq. (10) in the reciprocal space, we use the Bloch's theorem[17] and express the jth component of the displacement of an atom γ, $\mathbf{v}_{\gamma j}$, as

$$\mathbf{v}_{\gamma j} = (Nm/2)^{-1/2} \sum_{\mathbf{k}} A_j^1(\mathbf{k}) e^{i\mathbf{k}\cdot\mathbf{x}_\gamma^0}, \quad j=1,2,3, \quad \text{if } \gamma \in B_1, \tag{23}$$

and

$$\mathbf{v}_{\gamma j} = (Nm/2)^{-1/2} \sum_{\mathbf{k}} A_j^2(\mathbf{k}) e^{i\mathbf{k}\cdot\mathbf{x}_\gamma^0}, \quad j=1,2,3, \quad \text{if } \gamma \in B_2, \tag{24}$$

where $\mathbf{k}$ is the wave vector and for an N-atom silicon system, $\mathbf{k}$ takes $N/2$ distinct values,[18] and $A_j^t(\mathbf{k})$, $t=1,2$, are the unknown coefficients which are independent of the atom positions within a Bravais lattice. Substituting Eqs. (23) and (24) into Eq. (10), the Hamiltonian can be rewritten as

$$\begin{aligned} H = {} & U(\mathbf{x}^0) + \frac{1}{2}\sum_{\mathbf{k}} \sum_{t=1}^{2} \sum_{j=1}^{3} \dot{A}_j^{t*}(\mathbf{k}) \dot{A}_j^t(\mathbf{k}) \\ & + \frac{1}{2m} \sum_{\mathbf{k}} \sum_{t,s=1}^{2} \sum_{j,k=1}^{3} \sum_{\beta=1}^{N/2} \left. \frac{\partial^2 U(\mathbf{x})}{\partial \mathbf{x}_{\alpha j} \partial \mathbf{x}_{\beta k}} \right|_{\mathbf{x}=\mathbf{x}^0, \alpha \in B_t, \beta \in B_s} \\ & \cdot e^{i\mathbf{k}(\mathbf{x}_\beta^0 - \mathbf{x}_\alpha^0)} \cdot A_j^{t*}(\mathbf{k}) \cdot A_k^s(\mathbf{k}), \end{aligned} \tag{25}$$

where α denotes the center atom ($\alpha=1$) as shown in Figs. 2 and 3, and $\dot{A}_j^t(\mathbf{k})$ and $A_j^{t^*}(\mathbf{k})$ are the time derivative and complex conjugate of $A_j^t(\mathbf{k})$, respectively. Denoting $\partial^2 U(\mathbf{x})/(\partial \mathbf{x}_{\alpha j} \partial \mathbf{x}_{\beta k})|_{\mathbf{x}=\mathbf{x}^0, \alpha \in B_t, \beta \in B_s}$ as $\Phi_{j,k}^{ts}(\alpha,\beta)$, Eq. (25) can be rewritten in a matrix form as

$$\begin{aligned} H = {} & U(\mathbf{x}^0) + \frac{1}{2}\sum_{\mathbf{k}} [\dot{A}_j^{1*}(\mathbf{k}) \dot{A}_j^{2*}(\mathbf{k})] \begin{bmatrix} \dot{A}_j^1(\mathbf{k}) \\ \dot{A}_j^2(\mathbf{k}) \end{bmatrix} \\ & + \frac{1}{2}\sum_{\mathbf{k}} \left\{ [A_j^{1*}(\mathbf{k}) A_j^{2*}(\mathbf{k})] \frac{1}{m} \begin{bmatrix} \sum_{\beta=1}^{N/2} \Phi_{j,k}^{11}(\alpha,\beta) e^{i\mathbf{k}\cdot(\mathbf{x}_\beta^0 - \mathbf{x}_\alpha^0)} & \sum_{\beta=1}^{N/2} \Phi_{j,k}^{12}(\alpha,\beta) e^{i\mathbf{k}\cdot(\mathbf{x}_\beta^0 - \mathbf{x}_\alpha^0)} \\ \sum_{\beta=1}^{N/2} \Phi_{j,k}^{21}(\alpha,\beta) e^{i\mathbf{k}\cdot(\mathbf{x}_\beta^0 - \mathbf{x}_\alpha^0)} & \sum_{\beta=1}^{N/2} \Phi_{j,k}^{22}(\alpha,\beta) e^{i\mathbf{k}\cdot(\mathbf{x}_\beta^0 - \mathbf{x}_\alpha^0)} \end{bmatrix} \begin{bmatrix} A_k^1(\mathbf{k}) \\ A_k^2(\mathbf{k}) \end{bmatrix} \right\}, \quad j,k=1,2,3. \end{aligned} \tag{26}$$

Denoting $\mathbf{A}(\mathbf{k}) = [A_j^1(\mathbf{k}) A_j^2(\mathbf{k})]^T$, $j=1,2,3$, and the center matrix of the potential energy term in Eq. (26) as $\mathbf{D}(\mathbf{k})$, Eq. (26) can rewritten in a short form as

$$H = \frac{1}{2}\sum_{\mathbf{k}} \dot{\mathbf{A}}^H(\mathbf{k}) \dot{\mathbf{A}}(\mathbf{k}) + \frac{1}{2}\sum_{\mathbf{k}} \mathbf{A}^H(\mathbf{k}) \mathbf{D}(\mathbf{k}) \mathbf{A}(\mathbf{k}) + U(\mathbf{x}^0), \tag{27}$$

where $\mathbf{A}^H(\mathbf{k})$ is the Hermitian of $\mathbf{A}(\mathbf{k})$, and the 6×6 matrix $\mathbf{D}(\mathbf{k})$ is called the dynamical matrix. By diagonalizing the 6×6 Hermitian dynamical matrix $\mathbf{D}(\mathbf{k})$, the Hamiltonian given in Eq. (27) can be further written as

$$\begin{aligned} H &= \frac{1}{2}\sum_{\mathbf{k}} \dot{\mathbf{A}}^H(\mathbf{k}) \dot{\mathbf{A}}(\mathbf{k}) + \frac{1}{2}\sum_{\mathbf{k}} \mathbf{A}^H(\mathbf{k}) \mathbf{W}^H(\mathbf{k}) \mathbf{\Lambda}(\mathbf{k}) \mathbf{W}(\mathbf{k}) \mathbf{A}(\mathbf{k}) + U(\mathbf{x}^0) \\ &= \frac{1}{2}\sum_{\mathbf{k}} \dot{\mathbf{Q}}^H(\mathbf{k}) \dot{\mathbf{Q}}(\mathbf{k}) + \frac{1}{2}\sum_{\mathbf{k}} \mathbf{Q}^H(\mathbf{k}) \mathbf{\Lambda}(\mathbf{k}) \mathbf{Q}(\mathbf{k}) + U(\mathbf{x}^0), \end{aligned} \tag{28}$$

where $\mathbf{Q}(\mathbf{k}) = \mathbf{W}(\mathbf{k})\mathbf{A}(\mathbf{k})$ is the 6×1 vector of normal coordinates and $\mathbf{\Lambda}(\mathbf{k})$ is a 6×6 diagonal matrix whose components $\lambda_1(\mathbf{k}), \ldots, \lambda_6(\mathbf{k})$ are the eigenvalues of the dynamical matrix $\mathbf{D}(\mathbf{k})$. Equation (28) shows that the kinetic and the potential energy in the Hamiltonian are diagonalized simultaneously. Note that in Eq. (26), $\Phi_{j,k}^{11}(\alpha,\beta)$ and $\Phi_{j,k}^{22}(\alpha,\beta)$ involve interactions between atoms of the same Bravais lattice, and $\Phi_{j,k}^{12}(\alpha,\beta)$ and $\Phi_{j,k}^{21}(\alpha,\beta)$ represent interactions between atoms of different Bravais lattices. In the calculation of the dynamical matrix, for the center atom α, atom β loops over all the atoms in the system. However, as the Tersoff potential only includes the nearest neighbor interactions, it can be shown that $\Phi_{j,k}^{ts}(\alpha,\beta)$ has nonzero values only if the atom β is within two layers of atoms surrounding the center atom α, i.e., as shown in Figs. 2 and 3 for a given center atom α, β only needs to loop over the nearest 17 atoms (including the center atom) of atom α, i.e.,

$$\mathbf{D}(\mathbf{k}) = \frac{1}{m} \begin{bmatrix} \sum_{\beta=1,6,\ldots,17} \Phi_{j,k}^{11}(\alpha,\beta) e^{i\mathbf{k}\cdot(\mathbf{x}_\beta^0 - \mathbf{x}_\alpha^0)} & \sum_{\beta=2,\ldots,5} \Phi_{j,k}^{12}(\alpha,\beta) e^{i\mathbf{k}\cdot(\mathbf{x}_\beta^0 - \mathbf{x}_\alpha^0)} \\ \sum_{\beta=2,\ldots,5} \Phi_{j,k}^{21}(\alpha,\beta) e^{i\mathbf{k}\cdot(\mathbf{x}_\beta^0 - \mathbf{x}_\alpha^0)} & \sum_{\beta=1,6,\ldots,17} \Phi_{j,k}^{22}(\alpha,\beta) e^{i\mathbf{k}\cdot(\mathbf{x}_\beta^0 - \mathbf{x}_\alpha^0)} \end{bmatrix}, \quad j,k=1,2,3. \tag{29}$$

Note that, in $\Phi^{11}_{j,k}(\alpha,\beta)$ and $\Phi^{12}_{j,k}(\alpha,\beta)$, the center atom α belongs to the Bravais lattice B_1 as shown in Fig. 2, and in $\Phi^{21}_{j,k}(\alpha,\beta)$ and $\Phi^{22}_{j,k}(\alpha,\beta)$, α belongs to B_2 as shown in Fig. 3. The transformed Hamiltonian, Eq. (28), is the sum of the energies of $3N$ independent harmonic oscillators in **k**-space. The energy levels are given by

$$\epsilon_{n,\mathbf{k}s} = \frac{U(\mathbf{x}^0)}{3N} + \left(n+\frac{1}{2}\right)\hbar\omega_s(\mathbf{k}),$$
$$n = 0,1,2,\ldots, \quad s = 1,\ldots,6, \tag{30}$$

where **k** takes $N/2$ distinct values and $\omega_s(\mathbf{k}) = \sqrt{\lambda_s(\mathbf{k})}$, $s = 1,\ldots,6$, is the frequency of the sth oscillator for a given **k**. For a silicon crystal with dimensions $N_1\mathbf{a}_1$, $N_2\mathbf{a}_2$, and $N_3\mathbf{a}_3$ along the three axes and with the Born–von Karman boundary condition,[19] where $N_1 \times N_2 \times N_3 = N/2$ and $\mathbf{a}_1$, $\mathbf{a}_2$, and $\mathbf{a}_3$ are the three fcc Bravais lattice basis vectors, the allowed values of **k** are given by

$$\mathbf{k} = \frac{n_1}{N_1}\mathbf{b}_1 + \frac{n_2}{N_2}\mathbf{b}_2 + \frac{n_3}{N_3}\mathbf{b}_3, \quad n_1 = 1,\ldots,N_1,$$
$$n_2 = 1,\ldots,N_2, \quad n_3 = 1,\ldots,N_3, \tag{31}$$

where $\mathbf{b}_i$, $i=1,2,3$, are the basis vectors of the reciprocal lattice. The Helmholtz free energy of the system is computed as

$$A = U(\mathbf{x}^0) + \frac{1}{2}\sum_{\mathbf{k}}\sum_{s=1}^{6}\hbar\omega_s(\mathbf{k}) + k_BT\sum_{\mathbf{k}}\sum_{s=1}^{6}\ln(1-e^{-\hbar\omega_s(\mathbf{k})/(k_BT)}). \tag{32}$$

Due to the periodicity of the reciprocal lattice, **k** can be chosen to lie in the first Brillouin zone.[8] Furthermore, due to the point symmetry of the normal mode frequency $\omega_s(\mathbf{k})$, it is sufficient to evaluate $\omega_s(\mathbf{k})$ only in a small fraction of the first Brillouin zone.[20] This result can greatly reduce the computational effort required to calculate the free energy and other thermal properties of the silicon crystal. In this paper, as we compute the thermodynamic properties of the bulk silicon crystal, i.e., $N\to\infty$, **k** is taken as a continuous variable and $\Sigma_{\mathbf{k}}$ in Eq. (32) is replaced by an integral of **k**. Therefore, Eq. (32) can be rewritten as

$$A = U(\mathbf{x}^0) + \frac{1}{2}\int_{\mathbf{k}}\sum_{s=1}^{6}\hbar\omega_s(\mathbf{k})d\mathbf{k} + k_BT\int_{\mathbf{k}}\sum_{s=1}^{6}\ln(1-e^{-\hbar\omega_s(\mathbf{k})/(k_BT)})d\mathbf{k}. \tag{33}$$

The integration domain is chosen to be one quadrant of the first Brillouin zone which is decomposed into nine tetrahedrons as shown in Fig. 4. The integration is carried out by using Gaussian quadrature[21] for each tetrahedron.

For an N-atom system with the Born-von Karman boundary condition, the QHMK approach is mathematically equivalent to the QHM approach. However, due to the periodic and symmetric characteristics of the silicon lattice, one is able to reduce the size of matrix diagonalization from $3N\times 3N$ to 6×6, and confine the calculations within a fraction of the first Brillouin zone.

III. THERMAL PROPERTIES OF SILICON: MODEL EVALUATION

In this section, we calculate several thermodynamic properties of the Tersoff silicon by using the three quasiharmonic models described in Sec. II. In the QHM model, 64, 216, and 512 atoms which correspond to $2\times2\times2$, $3\times3\times3$ and $4\times4\times4$ unit cells, respectively, are used in the calculations. In addition, periodic boundary conditions are applied in the QHM model. The results are compared with the molecular dynamics (MD) data presented in Ref. 6.

A. Lattice constants

Thermal expansion coefficient as a function of temperature is a fundamental property of materials. It is well known that the classical harmonic approximation predicts no thermal expansion. Thermal expansion is indeed due to the anharmonic characteristics of the interatomic potential. As discussed in Sec. II, the quasiharmonic approximation, which accounts for the dependence of the phonon frequencies on the temperature, is a simple extension of the classical harmonic approximation. We compute the zero pressure lattice parameter $a(T)$ at various temperatures (0–1500 K) by using the three quasiharmonic models. The lattice parameter $a(T)$ is obtained when the Helmholtz free energy is minimized with respect to $a(T)$, i.e.,

$$\frac{\partial A}{\partial a} = 0. \tag{34}$$

Figure 5 shows the comparison of the computed lattice parameter with the MD results. The values computed from the QHMK model are in good agreement with the results from the MD simulations. However, the LQHM approach overestimates, by more than 50%, the variation of the lattice parameter with temperature. The lattice parameters obtained from the QHM model with 64, 216, and 512 atoms are also

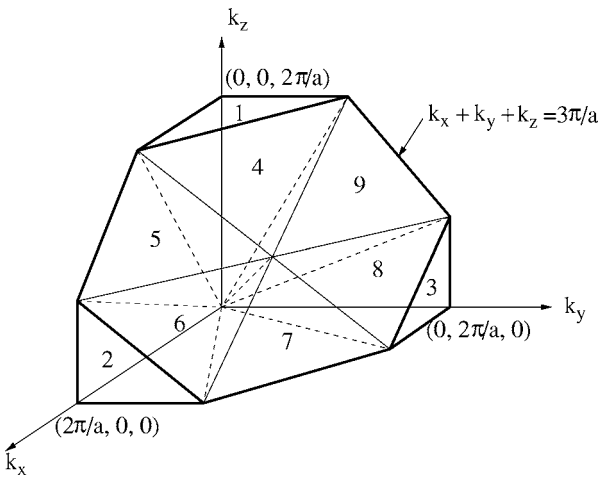

FIG. 4. A quadrant of the first Brillouin zone is decomposed into nine tetrahedrons.

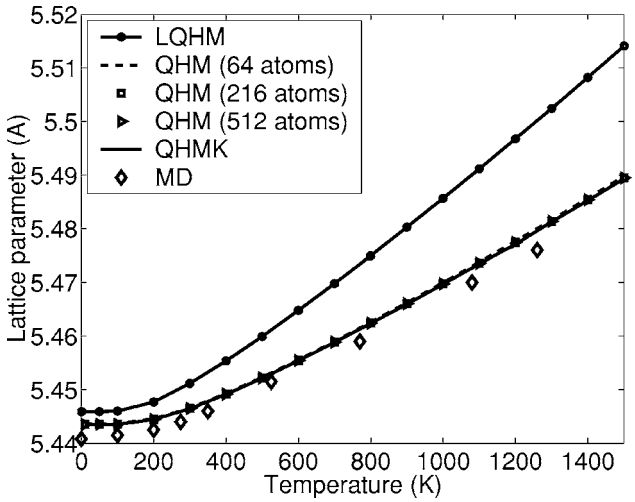

FIG. 5. Variation of the lattice parameter with temperature obtained from the LQHM approach, the QHM approach with 64, 216, and 512 atoms, the QHMK approach and MD (MD results are from Ref. 6).

in good agreement with the MD data. However, the CPU time of the QHM model is about 2, 90, and 1600 times higher than that of the QHMK approach for these cases, respectively. In addition, anharmonic effects become significant at high temperature as evidenced by the deviation between the QHMK approach results and the MD results at temperatures above 1000 K.

The thermal expansion coefficient c is defined by

$$c = \frac{1}{a}\frac{\partial a}{\partial T}. \tag{35}$$

The thermal expansion coefficient is obtained by fitting the simulation data shown in Fig. 5 with a fifth order polynomial of T. The comparison between the computed thermal expansion coefficients and the MD data is shown in Fig. 6. The LQHM approach predicts a much larger thermal expansion coefficient compared to the MD data. The QHMK and the QHM models give fairly accurate results for temperatures

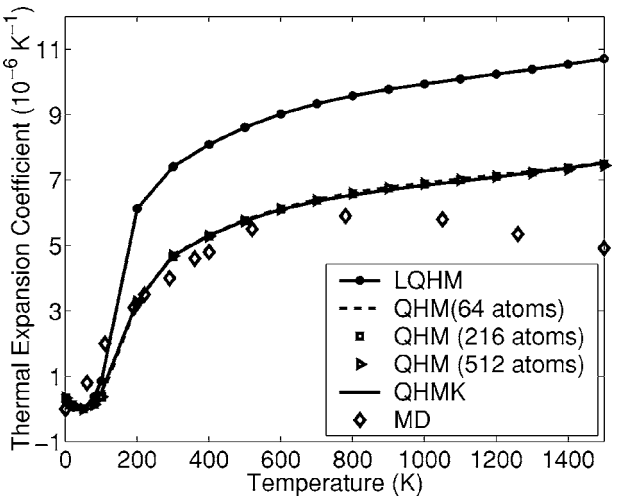

FIG. 6. Variation of the thermal expansion coefficient with temperature obtained from the LQHM approach, the QHM approach with 64, 216, and 512 atoms, the QHMK approach and MD (MD results are from Ref. 6).

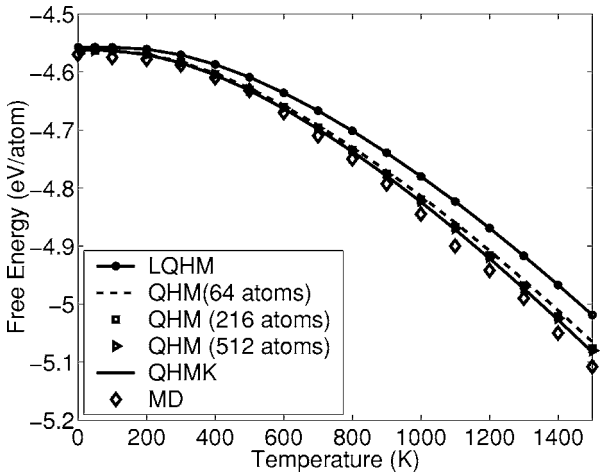

FIG. 7. Comparison of the Helmholtz free energy obtained from the LQHM, QHM with 64, 216, and 512 atoms, and the QHMK models with the MD data.

below 800 K. For higher temperatures, as anharmonic effects play an important role the deviation is significant.

B. Helmholtz free energy, internal energy, entropy, and heat capacity

Figure 7 shows the variation of the free energy with temperature obtained by using the three quasiharmonic models along with the MD simulation results. Note that all the MD results are from Ref. 6. As shown in Fig. 7, for low temperatures ($T<200$ K), the results from all the three methods are close to the MD results. However, for a temperature larger than 300 K, the results start to deviate. The results from the QHMK model are the closest to the MD data, the LQHM model results have the largest error compared to the MD data, and the QHM model results lie in between depending on the number of atoms used. The results from the QHM model converge to the QHMK results as the number of atoms increases. At 1500 K, the relative error between the QHMK and the QHM models with 64, 216, and 512 atoms is 0.35%, 0.12% and 0.05%, respectively. Since the results from the QHM model with 512 atoms are very close to the QHMK model results, they are not shown in Figs. 8–10. At higher temperatures, the error increases with all the quasiharmonic models indicating the significance of anharmonic effects.

After the Helmholtz free energy A is obtained, internal energy E, entropy S, and the heat capacity at constant volume C_v, can all be computed. The internal energy E is given by

$$E = A - T\frac{\partial A}{\partial T}. \tag{36}$$

The variation of the internal energy with temperature is shown in Fig. 8, where all the models give similar results. In this case, both the non-local effects and the anharmonic effects are quite small. Even at $T=1500$ K the error is within 0.004% of the MD results. Entropy, S, is a measure of the amount of energy in a physical system that cannot be used to

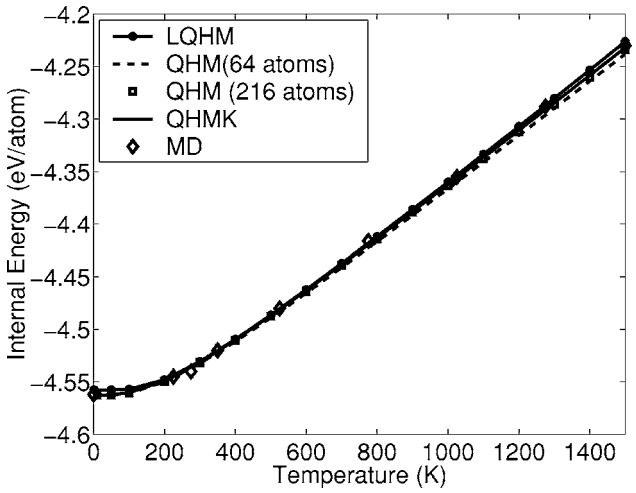

FIG. 8. Comparison of the internal energy obtained from the LQHM, QHM with 64 and 216 atoms, and the QHMK models with the MD data.

do work. It is also a measure of the disorder present in a system. S is computed by

$$S = \frac{E - A}{T}. \tag{37}$$

The LQHM approach considers each atom in the N atom system to be an isolated subsystem. It is well known that the entropy of a collection of N isolated systems is smaller than that of N interacting systems. For this reason, the entropy predicted by the LQHM model is lower compared to the MD data as shown in Fig. 9. The results obtained from the QHMK approach match well with the MD data for temperatures below 800 K. At 1500 K, the relative error of the LQHM and the QHMK models compared to the MD data is about 7.9% and 4.3%, respectively. The QHM model results lie in between the LQHM and the QHMK model results depending on the number of atoms used. The heat capacity C_v is given by

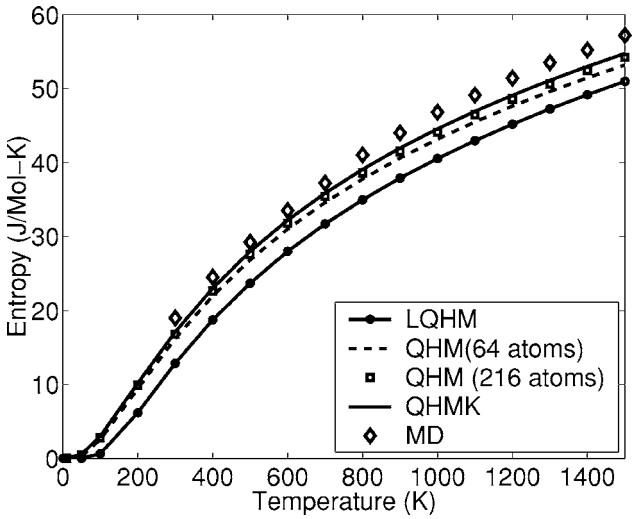

FIG. 9. Comparison of the entropy obtained from the LQHM, QHM with 64 and 216 atoms, and the QHMK models with the MD data.

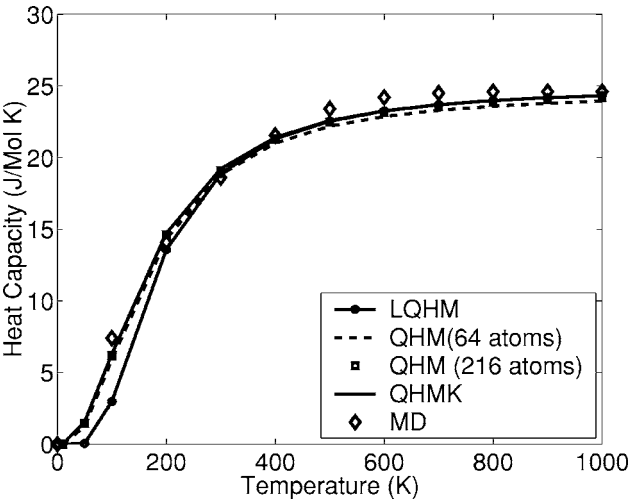

FIG. 10. Comparison of the heat capacity obtained from the LQHM, QHM with 64 and 216 atoms, and the QHMK models with the MD data.

$$C_v = -T\frac{\partial^2 A}{\partial T^2}. \tag{38}$$

The computed heat capacity is shown in Fig. 10. The LQHM approach underestimates the heat capacity at low temperatures ($<$150 K) while the QHMK approach shows a good match with the MD data.

The remarks are indicated as follows.

(1) The local quasiharmonic approximation is computationally attractive as it reduces the degrees of freedom by neglecting the correlations between the vibrations of different atoms. However, this computational efficiency is at the cost of the model's accuracy. As a result, the lattice constant, thermal expansion coefficient, Helmholtz free energy, and the entropy predicted by the local quasiharmonic model are in significant error compared to that of the MD data. Table I presents a comparison of the LQHM, QHM, and the QHMK models.
(2) The anharmonic effects are found to be significant at higher temperatures (typically $>$800 K) and the quasiharmonic models fail to capture the anharmonic effects.

IV. THERMAL PROPERTIES OF SILICON: STRAIN EFFECTS

The results in Sec. III indicate that the QHMK model gives the best results among the quasiharmonic models and the results from the QHM model approach the QHMK model results as the number of atoms increases. In this section, we study the strain effects on thermal properties of bulk silicon crystal by using both the QHM and the QHMK models. In particular, we compute the thermal properties when the silicon crystal is subjected to a compression, stretch and a shear deformation.

The silicon diamond structure contains two interpenetrating fcc lattices. As shown in Figs. 2 and 3, any given atom and its four nearest neighbor atoms belong to different Bravais lattices. When a perfect Bravais lattice is subjected

TABLE I. Comparison of the quasiharmonic models.

	LQHM	QHM		QHMK
Space	Real	Real		Reciprocal
Model	Local	Nonlocal		Nonlocal
Vibration correlations	No	Yes		Yes
Dimension of the force constant matrix	3×3	$3N\times3N$		6×6 for silicon
CPU time	$0.01s$	$0.2s$ (N=64)	$163s$ (N=512)	$0.1s$
Error in free energy at 1500 K (compared with MD results)	1.24%	0.84%	0.55%	0.49%

to a homogeneous deformation, the change in the atom positions is assumed to follow the Cauchy-Born rule,[15] i.e.,

$$\mathbf{x}_\beta^0-\mathbf{x}_\alpha^0=\mathbf{F}(\mathbf{X}_\beta^0-\mathbf{X}_\alpha^0)=\begin{bmatrix}F_{11}&F_{12}&F_{13}\\F_{21}&F_{22}&F_{23}\\F_{31}&F_{32}&F_{33}\end{bmatrix}(\mathbf{X}_\beta^0-\mathbf{X}_\alpha^0), \tag{39}$$

where $\mathbf{X}_\beta^0$ and $\mathbf{X}_\alpha^0$ are the equilibrium positions of atoms β and α, respectively, in the undeformed configuration and $\mathbf{F}$ is the deformation gradient of the Bravais lattice. Let $\mathbf{r}_{\alpha\beta}^0=\mathbf{x}_\beta^0-\mathbf{x}_\alpha^0$, $\mathbf{R}_{\alpha\beta}^0=\mathbf{X}_\beta^0-\mathbf{X}_\alpha^0$ be the vectors between the equilibrium positions of atoms α and β in the deformed and undeformed configurations, respectively. When the silicon crystal is subjected to a deformation, as the diamond structure contains two fcc Bravais lattices, an additional relative displacement can exist between the two fcc lattices. In this case, the Cauchy-Born rule gives

$$\mathbf{r}_{\alpha\beta}^0=\mathbf{F}\mathbf{R}_{\alpha\beta}^0+\boldsymbol{\xi}_j-\boldsymbol{\xi}_i,\quad \alpha\in B_i,\quad \beta\in B_j,\quad i,j=1,2, \tag{40}$$

where $\boldsymbol{\xi}_i$, $i=1,2$, are the additional inner displacements of the two Bravais lattices which can be determined by the energy minimization for a given deformation gradient $\mathbf{F}$. Since the inner displacements $\boldsymbol{\xi}_1$ and $\boldsymbol{\xi}_2$ are relative displacements between the two Bravais lattices, in order to rule out rigid-body translations we fix the lattice by setting $\boldsymbol{\xi}_2=0$. Therefore, $\boldsymbol{\xi}_2$ can be simply discarded. To simplify the notation, $\boldsymbol{\xi}_1$ is denoted as $\boldsymbol{\xi}$ in the rest of the paper. The Cauchy-Born rule can then be rewritten as

$$\mathbf{r}_{\alpha\beta}^0=\mathbf{F}\mathbf{R}_{\alpha\beta}^0+\boldsymbol{\xi}\quad \text{if } \alpha\in B_2 \text{ and } \beta\in B_1, \tag{41}$$

$$\mathbf{r}_{\alpha\beta}^0=\mathbf{F}\mathbf{R}_{\alpha\beta}^0-\boldsymbol{\xi}\quad \text{if } \alpha\in B_1 \text{ and } \beta\in B_2, \tag{42}$$

$$\mathbf{r}_{\alpha\beta}^0=\mathbf{F}\mathbf{R}_{\alpha\beta}^0\quad \text{if } \alpha,\beta\in \text{ same Bravais lattice}. \tag{43}$$

In the QHM approach, substituting Eqs. (39) and (41)–(43) into the force constant matrix, Eq. (9), the elements of the force constant matrix can be rewritten as a function of $\mathbf{X}^0$, $\mathbf{F}$, and $\boldsymbol{\xi}$, i.e.,

$$\Phi_{3\alpha+j-3,3\beta+k-3}=\left.\frac{\partial^2U(\mathbf{x})}{\partial\mathbf{x}_{\alpha j}\partial\mathbf{x}_{\beta k}}\right|_{\mathbf{x}=\mathbf{x}^0(\mathbf{X}^0,\mathbf{F},\boldsymbol{\xi})},\quad \alpha,\beta=1,\ldots,N,\quad j,k=1,2,3. \tag{44}$$

The eigenvalues of the force constant matrix [Eq. (44)], λ_j, $j=1,\ldots,3N$, are therefore functions of $\mathbf{F}$ and $\boldsymbol{\xi}$. Consequently, the frequencies of the harmonic oscillators and the Helmholtz free energy given in Eqs. (15) and (16), respectively, are also functions of $\mathbf{F}$ and $\boldsymbol{\xi}$. For a given temperature T and deformation $\mathbf{F}$, we first compute the lattice constant at temperature T for the undeformed crystal by using Eq. (34). Based on the computed lattice constant, the undeformed configuration of the crystal lattice, $\mathbf{X}^0$, at the given temperature T is obtained. The inner displacement $\boldsymbol{\xi}$ can then be calculated by minimizing the free energy with the given $\mathbf{F}$

$$\frac{\partial A}{\partial\boldsymbol{\xi}}=\frac{\partial U(\mathbf{x}^0)}{\partial\boldsymbol{\xi}}+\hbar\sum_{j=1}^{3N}\left(\frac{1}{2}+\frac{1}{e^{(\hbar\omega_j/(k_BT)}-1}\right)\frac{\partial\omega_j}{\partial\boldsymbol{\xi}}=0. \tag{45}$$

Equation (45) is solved by using the Newton's method.[22] Note that the derivatives of the eigenvalues ω_j shown in Eq. (45) can be calculated either analytically[23,24] or by using a numerical technique, e.g., the finite difference method.[22] After $\boldsymbol{\xi}$ is computed, ω_j can be calculated from the eigenvalues of the force constant matrix given in Eq. (44). The Helmholtz free energy and other thermodynamic properties can then be computed as discussed in the previous sections.

In the QHMK approach, from Eq. (39), it is easy to show that, in the reciprocal lattice of a Bravais lattice, a given wave vector $\mathbf{k}^0$ in the undeformed configuration deforms to $\mathbf{k}$ in the deformed configuration with the relation

$$\mathbf{k}=\mathbf{F}^{-T}\mathbf{k}^0. \tag{46}$$

Substituting Eqs. (39)–(46) into the dynamical matrix given in Eq. (29), one obtains

$$\mathbf{D}(\mathbf{k})=\frac{1}{m}\begin{bmatrix}\sum_{\beta=1,6,\ldots,17}\Phi^{11}_{j,k}(\alpha,\beta)e^{i\mathbf{k}^0\cdot\mathbf{R}^0_{\alpha\beta}} & \sum_{\beta=2,\ldots,5}\Phi^{12}_{j,k}(\alpha,\beta)e^{i\mathbf{k}^0\cdot(\mathbf{R}^0_{\alpha\beta}-\mathbf{F}^{-1}\boldsymbol{\xi})}\\ \sum_{\beta=2,\ldots,5}\Phi^{21}_{j,k}(\alpha,\beta)e^{i\mathbf{k}^0\cdot(\mathbf{R}^0_{\alpha\beta}+\mathbf{F}^{-1}\boldsymbol{\xi})} & \sum_{\beta=1,6,\ldots,17}\Phi^{22}_{j,k}(\alpha,\beta)e^{i\mathbf{k}^0\cdot\mathbf{R}^0_{\alpha\beta}}\end{bmatrix},\quad \alpha=1,\quad j,k=1,2,3, \tag{47}$$

where

$$\Phi^{ts}_{j,k}(\alpha,\beta)=\left.\frac{\partial^2 U(\mathbf{x})}{\partial\mathbf{x}_{\alpha j}\partial\mathbf{x}_{\beta k}}\right|_{\mathbf{x}=\mathbf{x}^0(\mathbf{X}^0,\mathbf{F},\boldsymbol{\xi}),\alpha\in B_t,\beta\in B_s},$$
$$j,k=1,2,3,\quad t,s=1,2. \tag{48}$$

Note that, $\boldsymbol{\xi}$ does not appear in the exponential term of the diagonal entries of the dynamical matrix shown in Eq. (47), where the atoms α and β belong to the same Bravais lattice. For a given $\mathbf{F}$, the inner displacement $\boldsymbol{\xi}$ is computed by

$$\frac{\partial A}{\partial\boldsymbol{\xi}}=\frac{\partial U(\mathbf{x}^0)}{\partial\boldsymbol{\xi}}+\hbar\int_{\mathbf{k}}\sum_{s=1}^{6}\left(\frac{1}{2}+\frac{1}{e^{\hbar\omega_s(\mathbf{k})/(k_BT)}-1}\right)\frac{\partial\omega_s(\mathbf{k})}{\partial\boldsymbol{\xi}}d\mathbf{k}=0. \tag{49}$$

Figure 11 shows the variation of the internal energy with temperature when the silicon crystal is under tension ($F_{11}>1$, $F_{22}=F_{33}=1$ and $F_{ij}=0$ for $i\neq j$) and compression ($F_{11}<1$) in the x direction ([100] direction). Figure 12 shows the results from both the QHM and the QHMK approaches. For all the calculations shown in this section, 512 atoms ($4\times4\times4$ unit cells) are employed in the QHM approach. All the results from the two approaches differ by less than 0.1%. For this reason, the QHM model results are not presented for the rest of the examples in this section. Figure 13 shows the variation of the Helmholtz free energy with temperature when the silicon crystal is under tension and compression. The variation of the internal energy and the free energy with tension and compression is asymmetric. It is largely due to the asymmetry of the Tersoff potential energy with tension and compression, i.e., when the distance between the atoms increases (tension), the potential energy increases slowly; whereas when the distance between the atoms decreases, the potential energy increases quickly. Therefore, the change in internal energy and free energy under an identical tension and compression state is different. In addition, at low temperatures, a compression state has higher internal energy compared to the tension state, while at high temperatures the situation is opposite.

Figure 14 shows the variation of the entropy with temperature for tension and compression of the bulk silicon crystal. While the entropy increases with temperature in all cases, the entropy of the system, when compared to the unstrained case, is lower when the silicon crystal is under compression and higher when the crystal is under tension. When the crystal is under tension (or compression), the volume of the crystal increases (or decreases) and the disorder of the system (entropy) increases (or decreases).

Figure 15 shows the tension/compression effect on the heat capacity. Heat capacity is an extensive thermodynamic variable which depends on the volume of the system. The volume change due to tension/compression changes the heat capacity at intermediate temperatures (150–800 K). It is well known that, as the temperature gets larger than the Debye temperature (625 K for silicon[8]), the heat capacity converges to a value close to $3k_B$ per atom regardless of the configuration. Therefore, at high temperatures ($\approx$1000 K), lattice deformation has little effect on the heat capacity as

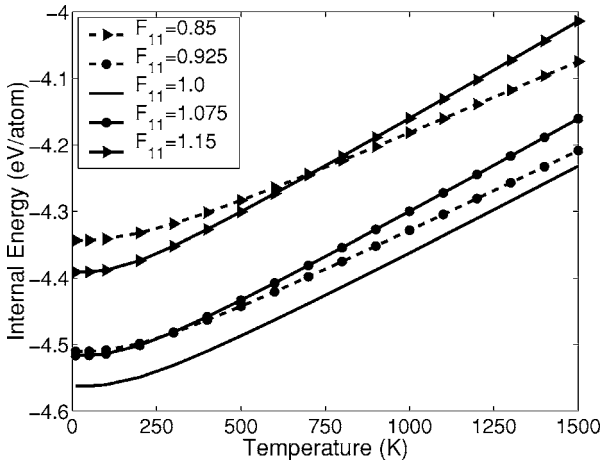

FIG. 11. Variation of the internal energy with temperature for tension ($F_{11}=1.075$, $F_{11}=1.15$) and compression ($F_{11}=0.925$, $F_{11}=0.85$) of a bulk silicon crystal. $F_{11}=1.0$ is the unstrained case.

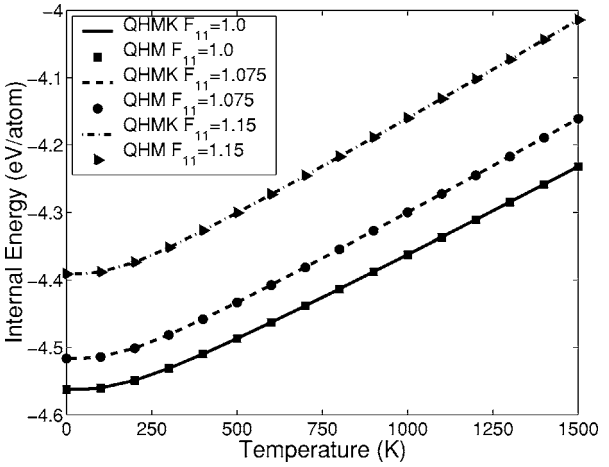

FIG. 12. Comparison of the internal energy obtained from the QHM model with 512 atoms and the QHMK model for tension ($F_{11}=1.075$, $F_{11}=1.15$) of a bulk silicon crystal. $F_{11}=1.0$ is the unstrained case.

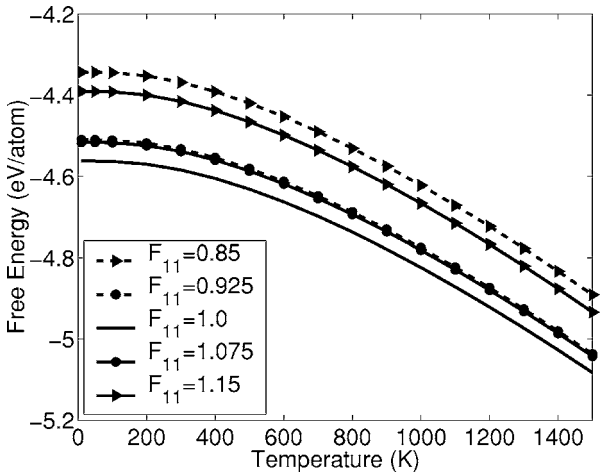

FIG. 13. Variation of the Helmholtz free energy with temperature for tension (F_{11}=1.075, F_{11}=1.15) and compression (F_{11}=0.925, F_{11}=0.85) of a bulk silicon crystal. F_{11}=1.0 is the unstrained case.

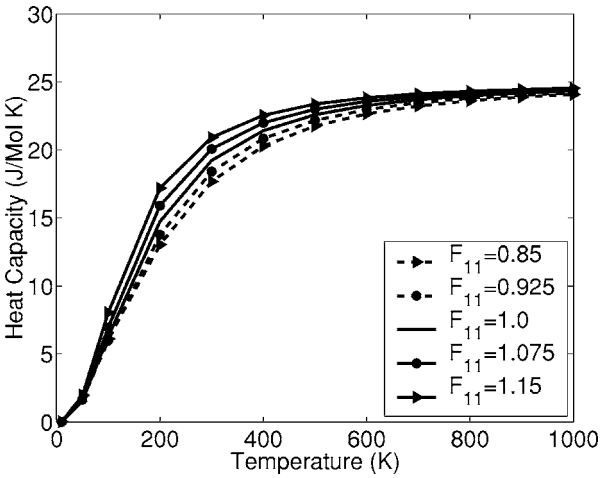

FIG. 15. Variation of the heat capacity with temperature for tension (F_{11}=1.075, F_{11}=1.15) and compression (F_{11}=0.925, F_{11}=0.85) of a bulk silicon crystal. F_{11}=1.0 is the unstrained case.

shown in Fig. 15. As the temperature decreases, both the value of the heat capacity and the variation of the heat capacity with strain approach zero.

Figures 16–19 show the variation of the thermodynamic properties under shear deformation. In contrast to the tension/compression state, due to the structure of the silicon lattice, the thermodynamic properties are symmetric with respect to F_{12} and F_{21}. In addition, changing the sign of the shear makes no difference to the thermal properties. Under shear deformation, some atoms move closer and the others move farther. This aspect along with the small volume change under shear deformation, gives rise to a smaller increase in the internal energy and the Helmholtz free energy, as shown in Figs 16 and 17. Furthermore, the volume change under shear is much smaller compared to the volume change under tension or compression. For this reason, the change in the entropy, shown in Fig. 18, and the change in the heat capacity, shown in Fig. 19, with shear is quite small.

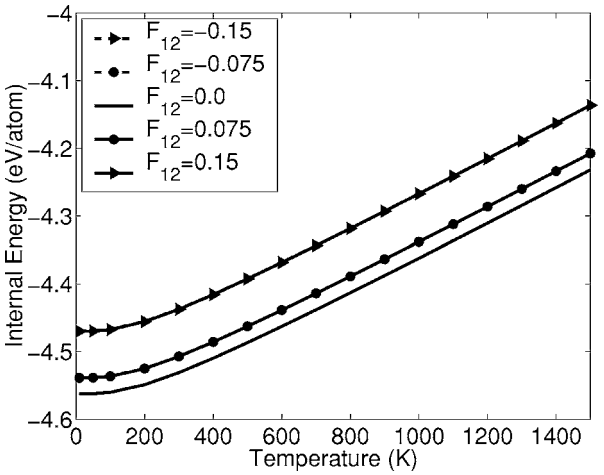

FIG. 16. Strain effect on the internal energy with shear deformation of $F_{12}=\pm0.15$, $F_{12}=\pm0.075$, and $F_{12}=0.00$.

V. CONCLUSIONS

In this paper, we assess the accuracy of various quasiharmonic models to compute thermodynamic properties of

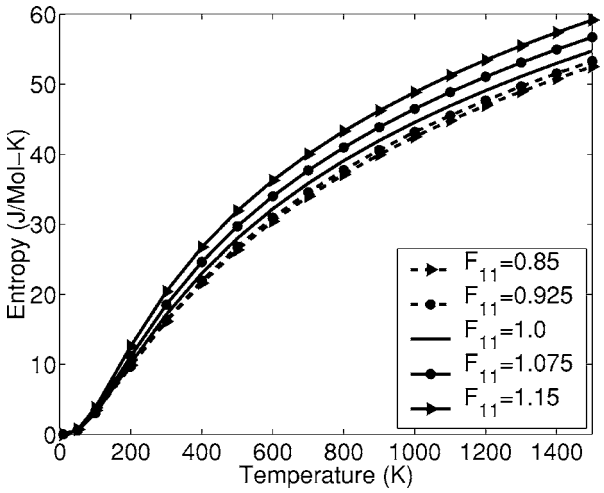

FIG. 14. Variation of entropy with temperature for tension (F_{11}=1.075, F_{11}=1.15) and compression (F_{11}=0.925, F_{11}=0.85) of a bulk silicon crystal. F_{11}=1.0 is the unstrained case.

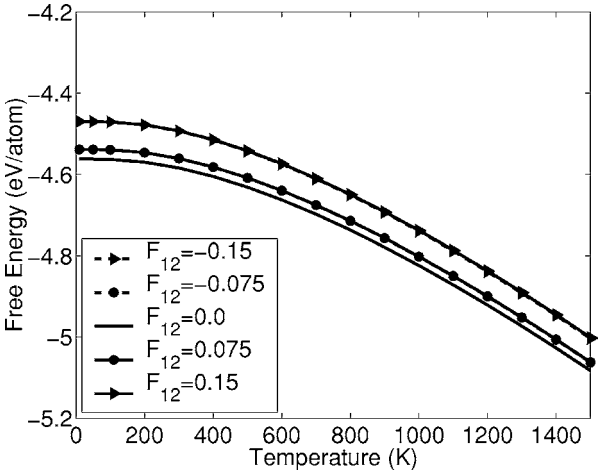

FIG. 17. Strain effect on the Helmholtz free energy with shear deformation of $F_{12}=\pm0.15$, $F_{12}=\pm0.075$, and $F_{12}=0.00$.

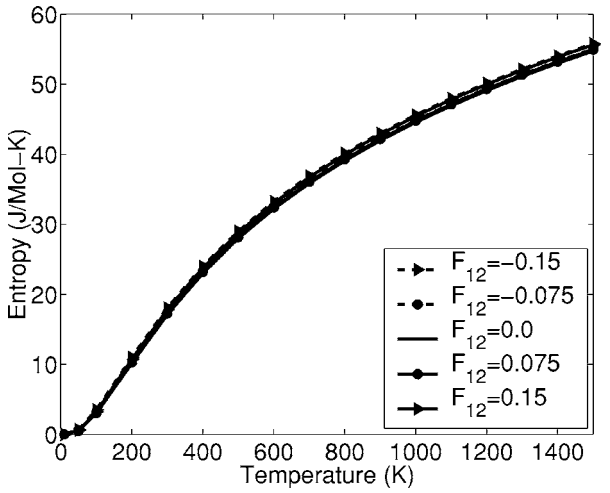

FIG. 18. Strain effect on entropy with shear deformation of $F_{12}=\pm 0.15$, $F_{12}=\pm 0.075$, and $F_{12}=0.00$.

bulk crystalline silicon described by the Tersoff interatomic potential. We show that the local harmonic model significantly overestimates the lattice constant and the thermal expansion coefficient, and underestimates the entropy of the silicon crystal compared to the MD data. The quasiharmonic model in the reciprocal space gives accurate results for temperatures up to 800 K. For higher temperatures, anharmonic effects become significant. When a sufficient number of atoms (>216) are used, the results obtained from the real space quasiharmonic model approach the QHMK model results, but with a significantly higher computational cost. In the second part of the paper, we compute the effect of the strain on the thermodynamic properties of silicon by using the QHM and the QHMK models. The thermodynamic properties vary significantly under a tension and a compression state and the variation under an identical tension and a compression deformation is asymmetric. Under a shear deformation, the thermal properties are symmetric as they do not vary with the direction of the shear. In addition, the effect of shear on the thermodynamic properties is small compared to the effect under tension/compression deformation.

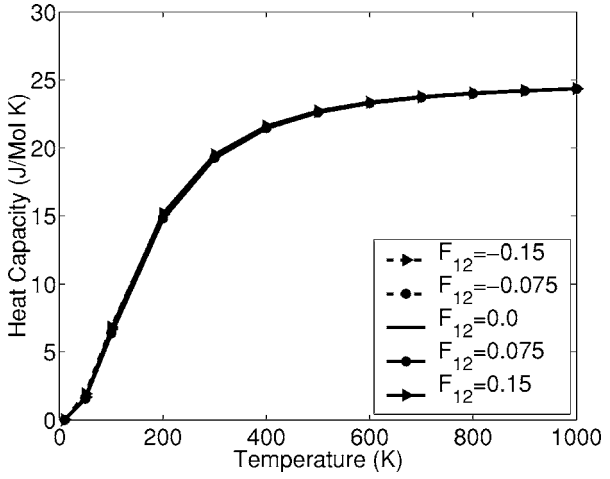

FIG. 19. Strain effect on the heat capacity with shear deformation of $F_{12}=\pm 0.15$, $F_{12}=\pm 0.075$, and $F_{12}=0.00$.

ACKNOWLEDGMENTS

We gratefully acknowledge support by the National Science Foundation under Grant Nos. 0103447, 0228390, 0403020, and 0519920. Two of the authors (H.Z. and Z.T.) are doctoral students at the Department of Mechanical and Industrial Engineering, UIUC. One of the authors (G.L.) is a research scientist at the Beckman Institute for Advanced Science and Technology.

[1] S. Wei, C. Li, and M. Y. Chou, Phys. Rev. B **50**, 14587 (1994).
[2] K. Karch, P. Pavone, W. Windl, D. Strauch, and F. Bechstedt, Int. J. Quantum Chem. **56**, 801 (1995).
[3] F. H. Stillinger and T. A. Weber, Phys. Rev. B **31**, 5262 (1985).
[4] J. Tersoff, Phys. Rev. B **38**, 9902 (1988).
[5] M. S. Daw and M. I. Baskes, Phys. Rev. Lett. **50**, 1285 (1983).
[6] L. J. Porter, S. Yip, M. Yamaguchi, H. Kaburaki, and M. Tang, J. Appl. Phys. **81**, 96 (1997).
[7] M. Karimi, H. Yates, J. R. Ray, T. Kaplan and M. Mostoller, Phys. Rev. B **58**, 6019 (1998).
[8] N. W. Ashcroft and N. D. Mermin, *Solid State Physics* (Harcourt, New York, 1976).
[9] A. A. Maradudin, E. W. Montroll, G. H. Weiss, and I. P. Ipatova, *Theory of Lattice Dynamics in the Harmonic Approximation* (Academic, New York, 1971).
[10] R. LeSar, R. Najafabadi, and D. J. Srolovitz, Phys. Rev. Lett. **63**, 624 (1989).
[11] M. L. Roukes, in *Technical Digest*, Solid-State Sensor and Actuator Workshop, Hilton Head, 2000, pp. 367–376.
[12] L. Pescini, H. Lorenz, and R. H. Blick, Appl. Phys. Lett. **82**, 352 (2003).
[13] Z. Tang, Y. Xu, G. Li, and N. R. Aluru, J. Appl. Phys. **97**, 114304 (2005).
[14] D. J. Griffiths, *Introduction to Quantum Mechanics* (Prentice-Hall, NJ, 2004).
[15] M. Born and K. Huang, *Dynamical Theory of Crystal Lattices* (Clarendon, Oxford, 1954).
[16] B. T. M. Willis and A. W. Pryor, *Thermal Vibrations in Crystallography* (Cambridge University Press, Cambridge, 1975).
[17] F. Bloch, Phys. Z. 52, 555 (1928).
[18] A. N. Cleland, *Foundations of Nanomechanics: From Solid-State Theory to Device Applications* (Springer-Verlag, Berlin, 2003).
[19] M. Born and T. von Karman, Phys. Z. **13**, 297 (1912).
[20] D. Brust, Phys. Rev. **134**, A1337 (1964).
[21] R. D. Cook, *Concepts and Applications of Finite Element Analysis* (Wiley, New York, 1989).
[22] M. T. Heath, *Scientific Computing: An Introductory Survey* (McGraw-Hill, New York, 1997).
[23] W. C. Mills-Curran, AIAA J. **26**, 867 (1988).
[24] U. Prells and M. I. Friswell, AIAA J. **35**, 1363 (1997).